IEEE Photonics Journal
An IEEE Photonics Society Publication

Open Access

Terahertz Polarization Splitters Based on Total and Partial Coupling in Dual Slotted Core Polymer Fiber: Comparison and Analysis

Volume 9, Number 3, June 2017

Hongzhi Chen
Guofeng Yan
Erik Forsberg
Sailing He, ***Fellow, IEEE***

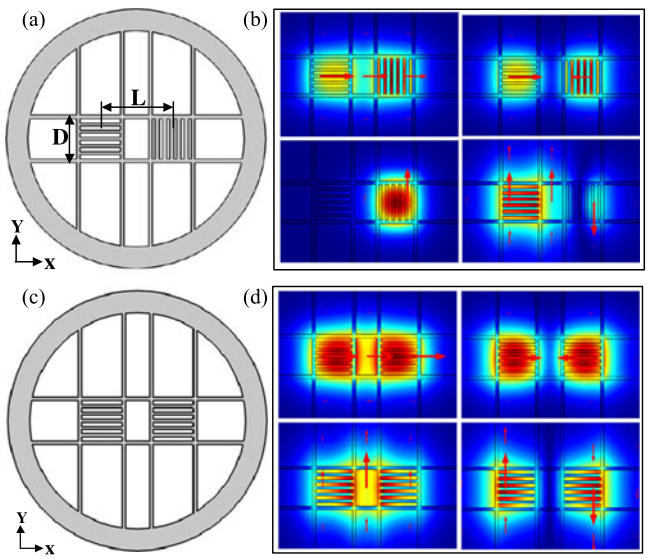

DOI: 10.1109/JPHOT.2017.2694886
1943-0655 © 2017 IEEE

IEEE photonics SOCIETY

IEEE

Terahertz Polarization Splitters Based on Total and Partial Coupling in Dual Slotted Core Polymer Fiber: Comparison and Analysis

Hongzhi Chen,[1] **Guofeng Yan,**[1] **Erik Forsberg,**[1] **and Sailing He,**[1,2] ***Fellow, IEEE***

[1]Centre for Optical and Electromagnetic Research, State Key Laboratory of Modern Optical Instrumentation, Zhejiang University, Hangzhou 310058, China
[2]Department of Electromagnetic Engineering, School of Electrical Engineering, Stockholm 10044, Sweden

DOI:10.1109/JPHOT.2017.2694886

Manuscript received March 29, 2017; accepted April 11, 2017. Date of publication April 18, 2017; date of current version May 3, 2017. This work was supported in part by the Program of Zhejiang Leading Team of Science and Technology Innovation under Grant 2010R50007, in part by the China Postdoctoral Science Foundation (No. 2015M571863), and in part by Zhejiang provincial Natural Science Foundation of China (LY14F010016). Corresponding author: Sailing He (e-mail: sailing@zju.edu.cn).

Abstract: Two terahertz (THz) polarization splitters based on dual slotted core polymer fiber are proposed and numerically investigated. The splitter structures are based on dual cores composed of subwavelength-scale air slots that are independently suspended within the fiber, which not only allows for single-mode propagation for the two orthogonal polarization modes with low absorption losses but enables them to couple with each other as well. Polarization splitters based on both symmetric and asymmetric dual slotted core structures, respectively, based on total and partial coupling are proposed and analyzed. The transmission modes, splitting lengths, and pertinent performance parameters of the two polarization splitters are investigated and numerically analyzed at a center-frequency of 1.0 THz. Comparisons of the two splitters with similar structural parameters are also carried out, which shows a comparably short splitting length of ∼1 cm and an ultra-low transmission loss of 0.4 dB with the asymmetric structure having a broader bandwidth and better extinction ratios.

Index Terms: Optical fiber devices, plastic optical fiber, polarization splitter, terahertz (THz).

1. Introduction

Terahertz radiation [1], which is located between microwaves and optical waves in the electromagnetic spectrum, has many potential applications in a large range of technical areas, such as infrared fingerprint spectral detection of explosives [2], biomedical imaging and tomography [3], label-free biological sensing [4], ultrasensitive THz-plasmonics gaseous sensing [5], and high speed and high data rate communications [6]. However, most dielectric materials have high absorption loss in the THz frequency range, which greatly complicates remote THz delivery. To suppress material absorption THz waveguide design, the key strategy is to maximize the fraction of power that is guided in dry air, which is almost transparent in the THz frequency range [7]. Many types of polymer waveguides have been designed and fabricated using relatively low absorption loss polymers (e.g., PE, Teflon,

and TOPAS), examples being subwavelength plastic fibers [8], porous fibers with subwavelength holes [7], [9], hollow core fibers with triangular lattices [10], honeycomb [11] photonic bandgap claddings, and THz surface-plasmon-coupled waveguide with 1-D photonic crystal structure [12]. Benefiting from the development of low-loss structures for THz polymer waveguides, some THz fiber devices have also been proposed and studied, such as THz fiber filters [13], [14] and THz fiber couplers [15], [16]. Functional THz fiber devices promise the development of an innovative field for compact and robust THz systems.

A fiber-based polarization splitter is one of the essential components in a THz system and to design an effective such, the operational bandwidth and transmission loss properties are key considerations. Due to the design flexibility, the compactness, and the outstanding performance of microstructured fibers, a lot of focus has been of developing dual-core fiber-based polarization splitters. Such designs can roughly be divided into two classes: symmetric coupler structures with two identical birefringent cores, and asymmetric couplers structure with non-identical cores. In the former, both parallel and perpendicular polarizations can be totally coupled between the two cores, albeit at different coupling lengths and thus, by manipulation of the transmission length, the two polarizations can be easily separated [17]–[19]. In the latter, only one polarization can be totally coupled between the two cores, while the coupling of the other polarization is effectively prohibited; the polarization splitting can thus be achieved by a single coupling process [20]–[22]. Recently, THz fiber polarization splitters based on microstructured dual-core photonic crystal fibers [23], two closely located porous fibers [24] and suspended dual rectangular core fibers [25], [26], have been reported. Porous core and photonic crystal cladding structures are effective for suppression of the absorption loss of the polymer material, however, the complicated structures makes actual fabrication challenging. To date, the realization of a simple structure polarization splitter with a short splitting length and low transmission loss remains a practical challenge.

In this paper, we present two THz fiber polarization splitters (PS) based on a symmetric and an asymmetric fiber coupler structure respectively. The guided mode of a polymer fiber with a single subwavelength-scale slotted core was first investigated, which showed a low absorption loss and a high birefringence property. Using the same core structure but extending this to a dual-core fiber, we find the fiber to exhibit strong polarization-dependent coupling behavior. A PS having two non-identical slotted cores supports total coupling between the two cores for only one of the two polarizations. Simulation results indicate that a 0.95 cm long splitter with an ultra-low loss of 0.26 dB, a high extinction ratio (ER) (better than -18 dB), and a bandwidth of 0.18 THz can be obtained at an operation frequency of 1.0 THz. For comparison, we also study a directional coupler with two identical slotted cores in which both of the two polarizations can be totally coupled between the two cores with different coupling lengths. Simulation results indicate that a 1.023 cm long splitter with a low loss of 0.32 dB, a high ER (better than -13 dB), and a bandwidth of 0.05 THz can be obtained at an operation frequency of 1.0 THz. Moreover, the outer polymer tube, serving as a protective enclosure to prevent undesirable external perturbation to the transmitted THz radiation, makes our configurations easier to manipulate and more suitable for real practical applications. The paper includes details of the design of the subwavelength-scale air slot core, simulation results on the characteristics of the two dual-core polarization structures, a comparison between the two structures, as well as a discussion on the possible fabrication methods.

2. Design of the Dual Slotted Core Polymer Fiber

2.1 Polymer fiber With Subwavelength Air Slot Core

As the basic structure of the dual-core fiber [see Fig. 5(a)], each suspended core can be considered as a single polymer fiber. To ensure high performance of polarization splitters to be proposed, each of the single cores need to display high birefringence and low material absorption loss. For this purpose we first design and analyze a polymer fiber with a single subwavelength-scale slotted core. Fig. 1 shows the schematic cross-section of the slotted core fiber. The core consists of six parallel air slots, supported by two parallel thin membranes extended in x- and y-directions with

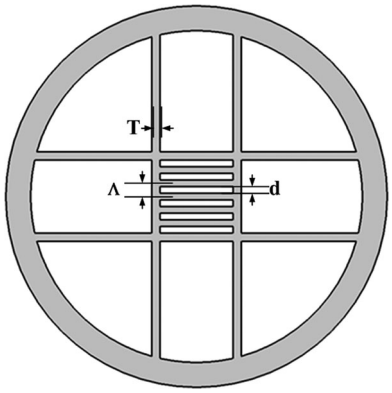

Fig. 1. Cross-section of the polymer fiber with a single suspended subwavelength-scale slotted core discussed in Section 2.1.

a height and thickness (T) of 3 mm and 20 μm, respectively. The outer large tube, which serves as a protective enclosure for the slotted core structure, has a diameter and thickness of 3.6 mm and 300 μm, respectively. In our study, the spacing distance Λ and height d of the air slots are 40 μm and 24 μm, respectively, yielding an air filling fraction, defined as $f = d/\Lambda$ is, to be 0.6. D is the core 'diameter' (technically the side length of the square shaped core), $D = 5\Lambda + \Lambda f + 2T$. The surrounding air serves as the fiber cladding. TOPAS, which is a nonpolar cyclic-olefin copolymer with a nearly constant refractive index of 1.53 in a broad THz frequency range, is used as the dielectric material of the fiber [27]. The frequency dependent absorption loss of bulk TOPAS is presented as blue-dashed line in Fig. 2(c). Bulk absorption loss is 0.7 dB/cm at 1.0 THz, and increases from 0.1 dB/cm to 2.5 dB/cm in the frequency from 0.8 THz to 1.4 THz.

The characteristics of the guided mode are obtained through the finite element method (FEM) with perfectly matched layer using commercial software COMSOL4.2. The computational region covers the whole fiber structure as shown in Fig. 1, including the slotted core, the supporting membranes and the outer polymer tube. The results are shown in Fig. 2 where we can see that due to the asymmetric structure of the slotted core, the x- and y-polarized modes exhibit high modal birefringence. As shown in Fig. 2(a), the dispersion curves of both x- and y-polarized modes increase with increasing frequency. A large birefringence of $\sim$0.047 occurs at 1.0 THz. The corresponding mode profiles in the core area are shown in the inset of Fig. 2(a) indicating a high polarization dependence. It is worth noting that the modal birefringence can reach a value of 0.04 for operation frequencies higher than 0.8 THz, which ensures short coupling lengths for directional coupling applications. In these calculations we simplified the slotted core fiber as a traditional circular step index fiber by using the radial effective index method. The accuracy and applicability of this method have been verified using the finite element method [28]–[30]. The single mode condition for a step-index fiber is determined by the normalized frequency V, which is expressed as

$$V = \frac{\pi D_{eff} f}{c} \sqrt{n_{eff}^2 - 1} \leq 2.405 \tag{1}$$

where $D_{eff} = \sqrt{2}D$ is the effective core diameter, f is the frequency, c is the speed of light in vacuum, and n_{eff} is the effective refractive index of the fiber core, which can be calculated by averaging the refractive indexes of the polymer material and air in a circle with the diameter D_{eff}. Thus the cut-off frequency can be calculated to be 1.2 THz, which actually should be even smaller due to the existence of dielectric strips in the cladding make the cladding index actually larger than 1 [30].

The fraction of the modal power in the air is an essential parameter for low loss THz waveguide for the obvious reason that, since dry air is a transparent medium for THz radiation, the straightforward way to suppress the absorption loss of polymer materials is to keep as large a fraction as possible

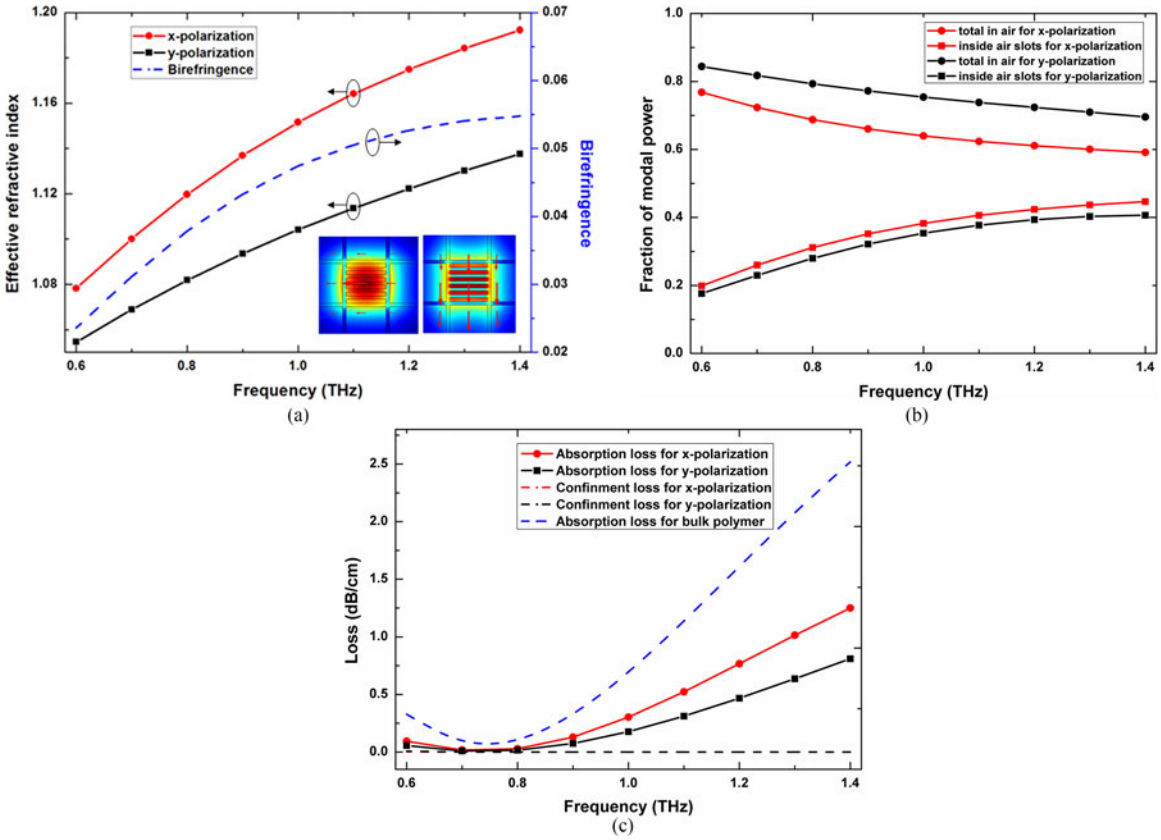

Fig. 2. Guided-mode analysis of the slotted core polymer fiber. (a) Dispersion curves and modal birefringence (Inset) Modal field profiles in the slotted fiber core for x- (left) and y- (right) polarizations at 1.0 THz, respectively. (b) Total fraction of the modal powers in air (air slots plus air cladding) and fraction in air slots only. (c) Effective material loss and confinement loss for x- and y-polarized modes, as well as the bulk polymer absorption loss as a function of frequency.

of the guided mode power in the air. Fig. 2(b) shows the total fraction of modal power in the air (i.e. in the air slots plus in the air cladding) as well as the fraction in the air slots only as a function of THz frequency. We can see that the total fraction of the modal power in the air monotonically decreases with increasing operation frequency, while the opposite is trend for the fraction in the air slots alone. In the other words, the propagation mode gradually transfers from the air regime outside the fiber core to strong confinement in the air slots inside the fiber core. This is because, at lower frequencies, the operation wavelength is far larger than the size of the fiber core, i.e., the fiber core acts as a subwavelength polymer fiber and the guided mode is in the subwavelength guidance regime. However, with increasing operation frequency, the wavelength becomes comparable in size to the slotted core and the confinement effect of the slotted core plays an increasingly important role thus confining the mode power more and more in the air slots. In a deep subwavelength guidance regime, the mode guidance will be very sensitive to the environment, and the light guidance can be easily lost due to leaky mode which can induce strong radiation [31]. The confinement loss in this fiber is caused by the power leakage through the polymer membranes between the slotted core and outer polymer tube. From a practical point of view, the designed polymer fiber should simultaneously display high birefringence and low material absorption loss, so the suitable operation frequency is around 1.0 THz, at which 64% and 75.4% of the x- and y-polarized modes distribute in the air, respectively. The effective material absorption loss α_{eff} of the guided fiber mode

can be calculated according to [32]:

$$\alpha_{eff} = \frac{(\varepsilon_0/\mu_0)\int_{polymer} n(r)\alpha_m(r)|E|^2 dA}{\mathrm{Re}\left(\int_{all} E \times H * \hat{z} dA\right)} \tag{2}$$

where ε_0 and μ_0 are the permittivity and the permeability in vacuum, respectively, and $n(r)$ and $\alpha_m(r)$ are the refractive index and material absorption loss of TOPAS, respectively. The confinement loss due to leaky mode also needs to be considered, and this can be derived from the imaginary part of the complex refractive index of the fundamental mode, with $\alpha_m(r)$ set to zero, to be:

$$\alpha_{con} = 2k\,\mathrm{Im}\left(n_{eff}\right) = \frac{4\pi f}{c}\mathrm{Im}\left(n_{eff}\right) \tag{3}$$

where c is the speed of light in vacuum, and Im (n_{eff}) is the imaginary part of the effective index of the guided mode

Fig. 2(c) shows the effective material loss and the confinement loss for x- and y-polarized modes as a function of frequency. We see that throughout the whole frequency range, the confinement loss is suppressed to a very low level, while the effective absorption loss increases significantly with frequency, which is due to the increase of the power fraction confined in the fiber material and the increase of the bulk polymer absorption loss [see the blue-dashed line in Fig. 2(c)]. Taking the x-polarized mode as an example: although the modal confinement value only reduces from 0.4 to 0.3 (a 25% reduction) as the operating frequency decreases from 1.4 THz to 0.8 THz, the more strongly frequency dependent material absorption which reduces from 2.52 dB/cm to 0.074 dB/cm (a 97% reduction). Furthermore, according to (2), we see that the effective absorption loss of the x-polarized mode reduces from 1.1 dB/cm to 0.025 dB/cm (a 77% reduction). For the confinement loss, there is an increasing trend when the operation frequency is below 0.6 THz. This is due to the fact mentioned above, i.e., that in this deep subwavelength guidance regime, the modal field becomes too large and is easily coupled to the leaky mode through the polymer membranes and outer polymer tube, resulting in an increased loss. At frequencies above 1.2 THz, the single mode operation ceases, and the fiber becomes multimode. Based on an overall consideration of the birefringence and absorption loss, the operation frequency of the proposed structure is chosen as 1.0 THz. It is, however, obviously possible to, by modifying the parameters of the slotted core, easily tune the optimal operation frequency.

2.2 Dual Slotted Core Polymer Fiber

Above we demonstrated that a slotted core polymer fiber can achieve low absorption loss and high birefringence. By extending the single slotted core polymer fiber to a dual core structure, we can easily realize a polarization splitter. Fig. 5(a) shows the schematic cross-section of our proposed dual slotted core fiber, which we label Splitter-1. This consists of two asymmetrical slotted cores A and B. In our design, we optimize the parameters of two slotted cores to minimize the transmission loss of the device. For a polarization splitter with lossless or low loss material, achieving a ratio of coupling lengths for the x- and y-polarization to be 1/2 or 2/3 could also be used as a design method. However, for a THz polarization splitter, the material absorption loss is high and due to this a primarily design aim is for the length of the splitter as short as possible and as using the coupling length ratio as a design criteria may not yield the shortest coupling length, the lowest transmission loss can not be guaranteed.

We design the dual core fiber using the Index Converse Matching Coupling (ICMC) method [23]. The dual slotted core fiber is in essence a combination of two single slotted core fibers A and B with the core distance $L = \rho D$, where D is the core diameter and ρ is defined as the normalized core separation, here set to $\rho = 1.5$. The core areas of the fibers A and B are shown in Fig. 3, with fiber A has the same parameters as the that proposed and discussed in the Section 2.1. We should adopt two steps to adjust the dispersion curves of fiber A for that of fiber B by using the ICMC method, namely rotating and overlapping. I.e. fiber B is obtained by firstly rotating fiber A by 90 degrees and secondly by decreasing the parameter d_B of the air slots until the x-polarized mode

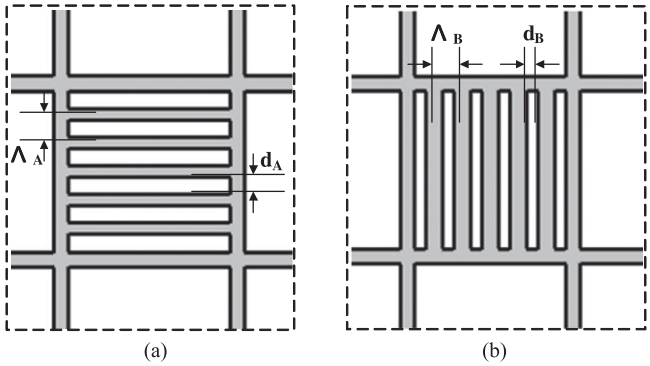

Fig. 3. Cross-section of core areas of suspended slotted core fibers A and B.

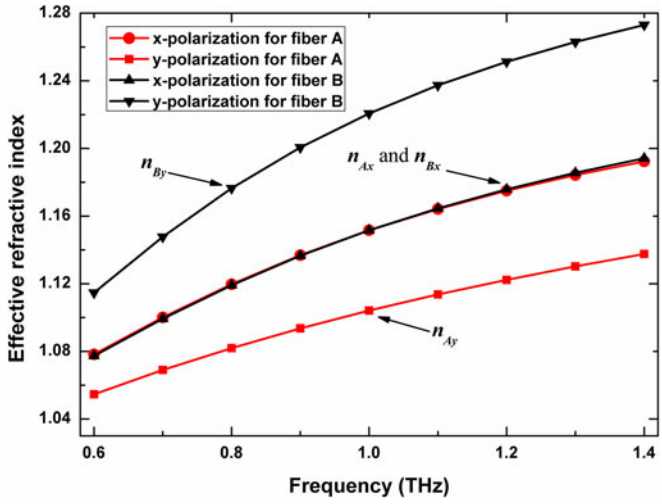

Fig. 4. Dispersion curves for fibers A and B obtained by using the ICMC method discussed in Section 2.2.

dispersion curve for fiber B overlaps with that of fiber A (see Fig. 4). Thus, the core parameters of the fiber B are $\Lambda_B = \Lambda_A = \Lambda = 40\,\mu$m and $d_B = 16.16\,\mu m$, and the air filling fraction of the fiber B is $f_B = d_B/\Lambda_B = 0.404$.

Fig. 4 shows the dispersion curves of fibers A and B designed above. n_{Ai} and n_{Bi} are defined as the effective refractive index of the i-polarized mode of the suspended single slotted core fibers A and B. We can see that the condition $n_{Ax} = n_{Bx}$ can be satisfied throughout the operation frequency band. Thus, coupling between the x-polarized modes of the two fibers can be realized, while at the same time coupling between the y-polarized modes is effectively prohibited due to the large effective refractive index difference between them. Fig. 5(b) shows the electric field distributions of the even and odd supermodes for the x- and y-polarizations in the dual slotted core fiber at 1.0 THz. The even and odd supermodes are superpositioned of the individual single core modes, which have symmetric and anti-symmetric electric field distributions. It is clear that, in the dual slotted core fiber, there is a strong coupling between the x-polarized even and odd modes, while the coupling behavior of the y-polarized modes is very weak. Consequently, a polarization splitter based on partial coupling of the two orthogonal polarizations can be achieved.

For comparison, we also propose another polarization splitter based on dual slotted core fiber, which we label Splitter-2. Splitter-2 has a symmetric coupling structure, which we obtain by combining two identical fibers A into a dual core structure with the same core separation L, as Splitter-1 [see Fig. 5(c)]. Fig. 5(d) shows typical electric field distributions of the four transmission

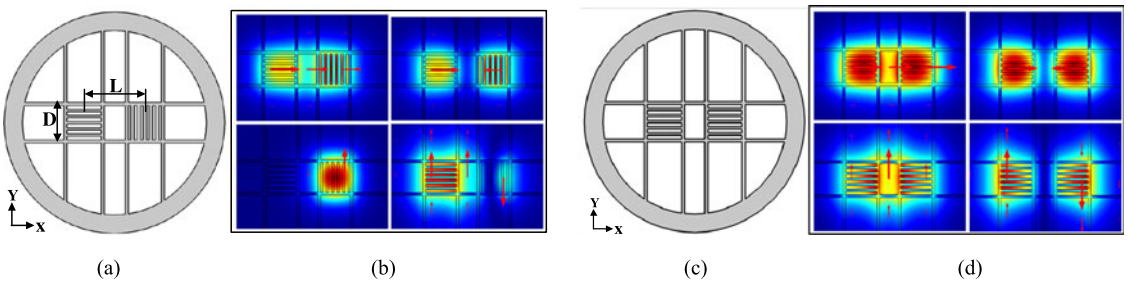

Fig. 5. (a) Cross-section and (b) electric field distributions of the four transmission supermodes of Splitter-1 with $\Lambda = 40\,\mu$m, $f_A = 0.6$, $f_B = 0.404$, and $\rho = 1.5$ at 1.0 THz. (c) Cross-section and (b) electric field distributions of the four transmission supermodes of the Splitter-2 with $\Lambda = 40\,\mu$m, $f = 0.6$, and $\rho = 1.5$ at 1.0 THz.

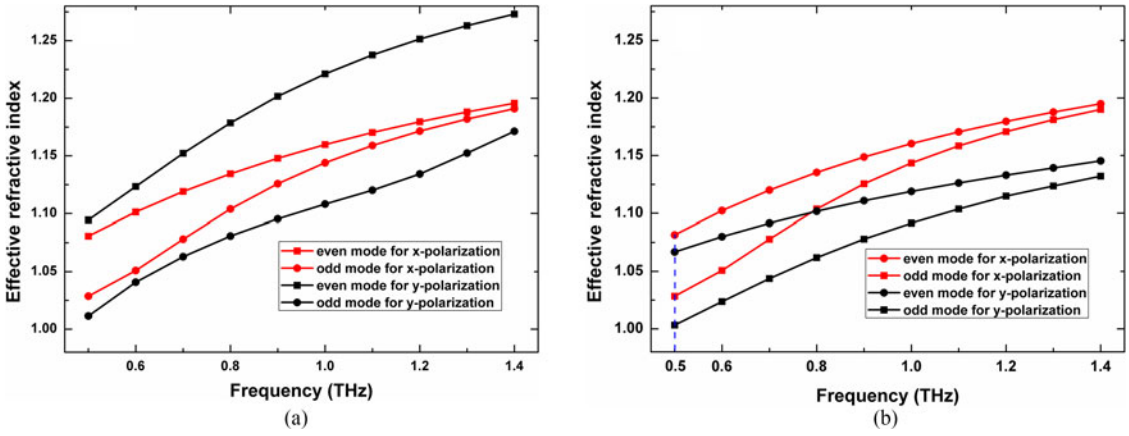

Fig. 6. Dispersion curves of the four supermodes for the Splitter-1 (a) and Splitter-2 (b) as a function of frequency.

supermodes of Splitter-2 at 1.0 THz. Although both the x- and y-polarized states can be totally coupled between the two cores of Splitter-2, the two polarization states have different coupling lengths due to the high birefringence of the slotted core structure. The two polarizations can therefore be easily separated at certain propagating distances making a polarization splitter based on total coupling possible by choice of the transmission length.

Fig. 6(a) and (b) shows numerically calculated dispersion curves of the four transmission supermodes of Splitter-1 and Splitter-2. We see the same trend for all the dispersion curves of the two splitters in that they increase with frequency in the range around the operating frequency of 1.0 THz. For Splitter-1, the effective refractive index difference for x-polarized supermodes is obviously smaller than that of y-polarized supermodes, while that difference for the two polarized supermodes is comparable for Splitter-2. According to mode coupling theory, the maximum coupling efficiency for x- and y-polarizations can be calculated though use of (4) [33]

$$\eta_i = \frac{\kappa_i^2}{\kappa_i^2 + \delta_i^2} = \frac{\left(n_e^i - n_o^i\right)^2}{\left(n_e^i - n_o^i\right)^2 + \left(n_{Ai} - n_{Bi}\right)^2}, i = x, y \tag{4}$$

where κ is defined as the coupling coefficient, and δ_i is defined as the phase mismatch constant for i-polarization. $\kappa_i = \frac{\beta_e^i - \beta_o^i}{2} = \frac{\pi}{\lambda}(n_e^i - n_o^i)$, where β_e^i and β_o^i are the propagation constants of i-polarized even and odd modes, respectively. n_e^i and n_o^i are the effective refractive indices of i-polarized even and odd modes, respectively.

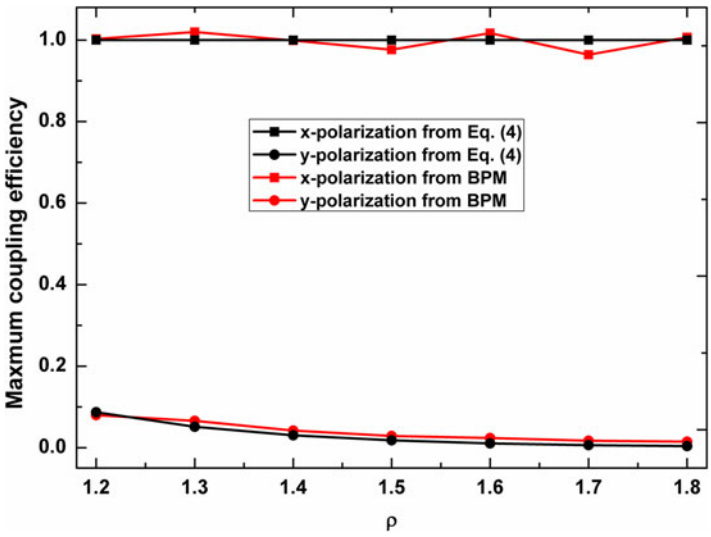

Fig. 7. Maximum coupling efficiencies of the x- and y-polarized supermodes for Splitter-1 as a function of the normalized core separation ρ derived both from (4) and a BPM simulation.

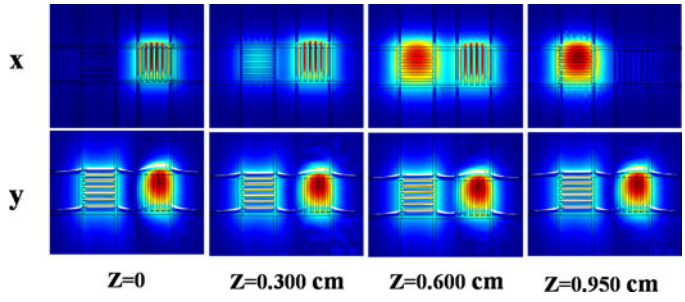

Fig. 8. Electric field distributions of the x- and y-polarized modes in Splitter-1, at z = 0, 0.300 cm, 0.600 cm, and 0.950 cm, respectively. Top and bottom rows correspond to the x- and y-polarized modes, respectively.

Fig. 7 shows the maximum coupling efficiency of the x- and y-polarizations for Splitter-1 as a function of the normalized two core distances ρ. It shows that the maximum coupling efficiency is close to 100% for the x-polarized supermodes, while for the y-polarization supermodes, it decreases from 10% to nearly zero as the ρ value increases from 1.2 to 1.8. To verify the calculated results of maximum coupling efficiency from (4), a 3-D model was built with the parameters above by using a full vectorial beam propagation method (BPM) based on FEM with an anisotropic perfectly matched layers boundary condition. Fig. 8 shows the transmission evolution of the x- and y-polarized modes in the two cores of the splitter, depicting the distribution of both polarizations at z = 0, 0.300 cm, 0.600 cm, and 0.950 cm. We can see that the x-polarized mode is almost completely coupled from one core to the other in one coupling length, while most of the y-polarized mode remains in one core. These simulation results of the maximum coupling efficiency are also shown in Fig. 7 and the results agree well with those calculated according to (4). I.e. only the x-polarized supermodes exhibit strong coupling behavior, and the coupling between the y-polarized supermodes is effectively prohibited. For Splitter-2, the maximum coupling efficiency for the two polarizations are both 100% since the x- and y-polarized modes of fibers A and B are both index-matched in the symmetric dual core structure.

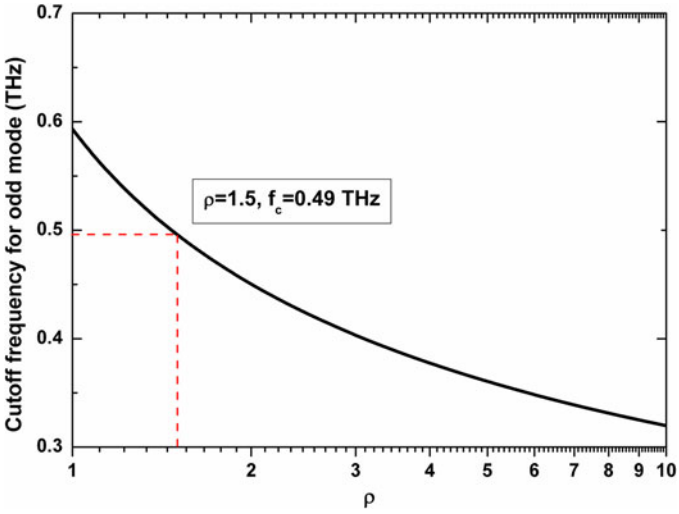

Fig. 9. Cutoff frequency of the odd mode of Splitter-2 as a function of the normalized core separation ρ.

It is known from mode coupling theory that in a symmetric directional coupler, the even mode always exists, but there is a cutoff frequency for the anti-symmetric mode or odd mode, which can be estimated by in an asymptotic form to be [34]

$$f_c \approx \frac{\left\{\frac{8}{[1+4\ln(2\rho)]}\right\}^{1/2} c}{\pi D_{eff}\left(n_{eff}^2 - 1\right)^{1/2}}. \tag{5}$$

In order to achieve a high extinction ratio in polarization splitting applications, one should ensure the existence of the odd modes. For example, in [15], the operation frequency of a two-fiber-based coupler is below the cutoff frequency of the odd mode, making the even mode the only guided mode however the fact that there is no oscillation behavior between the two fibers leads to severe crosstalk for the coupler. In contrast, for our symmetric dual slotted core fiber, i.e., Splitter-2, the cutoff frequencies for the x- and y-polarized odd modes are the same because of the square shape of the fiber cores. Fig. 9 plots the cutoff frequency of the odd mode as a function of the normalized core separation ρ. We can see that the calculated cutoff frequency for the odd mode is about 0.49 THz (as indicated by red dashed line in Fig. 9) for $\rho = 1.5$. As a validation for this approximation, we examine the dispersion curves of the splitters at $\rho = 1.5$ in Fig. 6, and find the cutoff frequency of Splitter-2 to be 0.5 THz [indicated by the blue dashed line in Fig. 6(b)]. There is a very small discrepancy between the calculation value (0.49 THz) and the simulated value (0.50 THz), which is reasonable. This as, due to the existence of the dielectric strips in the cladding, the cladding index is actually larger than 1, so the actual cutoff frequency should slightly larger. Thus, as the working frequency for our designed Splitter-2 is 1.0 THz, the odd modes of both polarization directions are well supported. Meanwhile, it still allows us to optimize the proposed splitter by modifying ρ in a reasonable range (see Section 3.2 for further discussion).

3. Performance Characterizations of the Proposed Polarization Splitters

3.1 Coupling

Coupling behavior can be characterized by use of the even and odd supermodes. For each polarization the coupling length is the basic parameter, which is defined as the length required to achieve

a phase change π between the even and odd modes and which can be calculated as [11]

$$L_c^i = \frac{\pi}{\beta_e^i - \beta_o^i} = \frac{\lambda}{2\left(n_e^i - n_o^i\right)}, i = x, y \tag{6}$$

where β_e^i and β_o^i are the propagation constants of i-polarized even and odd modes, respectively; n_e^i and n_o^i are the effective refractive indices of i-polarized even and odd modes, respectively.

The transmission loss is also a key feature for evaluation of the performance of polarization splitters in the THz regime. This is mainly derived from the material absorption of the THz radiation and the leakage of the mode field to infinity, i.e. the confinement loss. In Section 2.1, we showed that at an operation frequency of 1.0 THz, the confinement loss is nearly zero and thus in our simulation, the transmission loss T_{loss} can be expressed as

$$T_{loss}^i = L_s \times \alpha_{eff}^i, i = x, y \tag{7}$$

where α_{eff}^i is the effective material absorption loss of the i-polarized mode $i = x, y$. Noting that the polarized light beam propagates in the fiber by the way of supermode-coupling, α_{eff}^i is here considered to be the average value of the effective material absorption loss of the even and odd modes for the corresponding i-polarization direction.

The coupling behavior of the dual core fiber can be simulated based on the directional coupling theory. Numerical calculations was first carried out based on the four simulated supermodes with $\Lambda = 40\,\mu$m, $f_A = 0.6$, $f_B = 0.404$, $\rho = 1.5$ at 1.0 THz [see Fig. 5(b)] for Splitter-1. When a fundamental mode with power of P_{in} is launched into core A, the output power from core A ($P_{out,A}$) and core B ($P_{out,B}$) can be expressed as follows [35]:

For core A:

$$P_{out,A}^x = P_{in}^x \cdot \eta_x \cdot \cos^2\left(\frac{\pi z}{2L_C^x}\right) \cdot \exp\left(-\alpha_{loss}^x z\right) \tag{8}$$

$$P_{out,A}^y = P_{in}^y \left[\left(1 - \eta_y\right) + \eta_y \cdot \cos^2\left(\frac{\pi z}{2L_C^y}\right) \cdot \exp(-\alpha_{loss}^y z)\right]. \tag{9}$$

For core B:

$$P_{out,B}^x = P_{in}^x \cdot \eta_x \cdot \sin^2\left(\frac{\pi z}{2L_C^x}\right) \cdot \exp(-\alpha_{loss}^x z) \tag{10}$$

$$P_{out,B}^y = P_{in}^y \cdot \eta_y \cdot \sin^2\left(\frac{\pi z}{2L_C^y}\right) \cdot \exp(-\alpha_{loss}^y z) \tag{11}$$

where z is the propagation length.

The normalized transferred power of x- and y-polarized modes along the propagation distance in core A is illustrated in Fig. 10(a) when the THz radiation was launched into core A. We can see that the power of the x-polarized mode changes periodically in core A as a result of its coupling with core B. However, the power of the y-polarization mode just shows a tiny fluctuation, and most of the power remains in core A. Thus, separation of the two polarizations can be achieved in one coupling length of the x-polarization (indicated by the red dashed line), which is the splitting length of Splitter-1, and which here is 0.950 cm.

The coupling behavior of the Splitter-2 can also be calculated by (8)–(11) by setting $\eta_x = \eta_y = 1$. We also carried of a numerical calculation for Splitter-2 with parameters $\Lambda = 40\,\mu$m, $f = 0.6$, $\rho = 1.5$ at 1.0 THz [see Fig. 5(d)]. The normalized power transformation of x- and y-polarized modes along the propagation distance in core A is illustrated in Fig. 10(b). We can see that the power of each polarization mode changes periodically in core A, and due to high birefringence of the dual slotted core fiber, the coupling lengths L_c^x and L_c^y are different and are determined to be 0.893 cm and 0.551 cm, respectively [see Fig. 10(b)]. In this case, the splitting length L_s is a selected length at which the powers of the x- and y-polarized modes have the first maximum value difference. As indicated by the red dashed line marked in Fig. 10(b), the two polarizations are effectively separated from each other at a separation distance L_s of 1.023 cm.

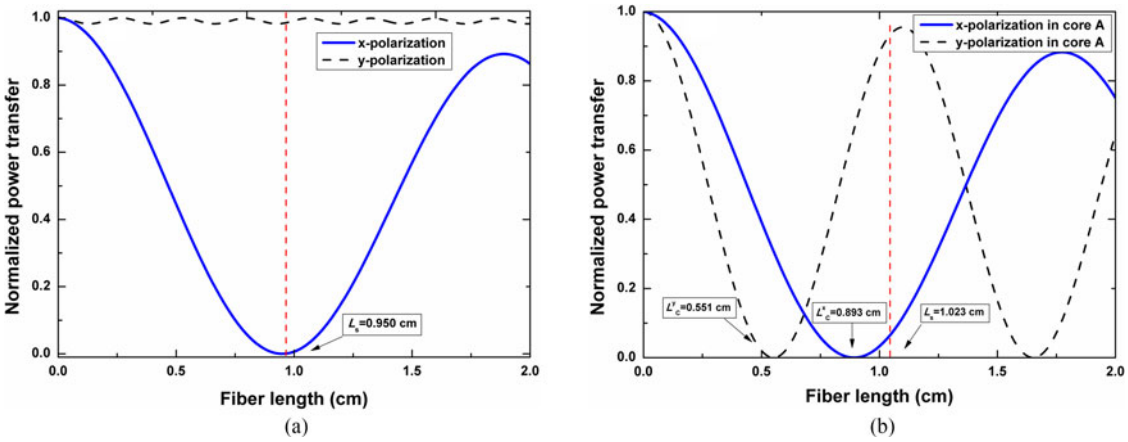

Fig. 10. (a) Normalized power transfer of x- and y-polarization as functions of fiber length for Splitter-1 in core A. (b) Normalized power transfer of x- and y-polarization as functions of fiber length for Splitter-2 in core A.

3.2 Transmission Loss

In order to compare the performances of the two splitters, we keep $\Lambda = 40\,\mu$m, $f_A = 0.6$, $f_B = 0.404$ for Splitter-1and $\Lambda = 40\,\mu$m, $f = 0.6$ for Splitter-2. By adjusting the normalized core separation ρ, the transmission losses of the two polarization splitters are investigated.

Fig. 11(a) shows the splitting length for the two splitters at 1.0 THz as ρ increases from 1.2 to 1.8. The results indicate that, for Splitter-1, the splitting length L_s increases with the increasing ρ, which is a result of a decrease of the overlap between the two x-polarization supermodes. For Splitter-2, the splitting length L_s does not display a monotonic change, which is determined by the selection process of the transmission length based on the total coupling principle as discussed in Section 3.1. When ρ is between 1.5 or 1.8, the splitting length is about two times L^x_c, however when ρ decreases to 1.4, the splitting length increases to about three times L^x_c. This is due to the fact that the difference between the x- and y-coupling lengths is getting smaller, a longer transmission length is needed to realize the splitting of two polarizations. Fig. 11(b) shows the effective material absorption loss α^j_{eff} as a function of ρ. We find that for both x- and y-polarized modes, the effective material absorption loss α^j_{eff} decreases gradually with increasing ρ; the relatively large decreasing trend of the y-polarized mode for Splitter-1is due to the fact that the y-polarized mode power is mostly confined to one of the cores and its surrounding air region, while the x-polarized mode is distributed across both cores and the corresponding air regions. With increasing ρ the distance between the two cores becomes large, which only affects the mode field position for the x-polarized mode but the obvious decrease of polymer material in the surrounding air region of one core for the y-polarized mode. Thus, there is a relatively large decrease of the material absorption loss for the y-polarized mode but little decrease of that for x-polarized mode for Splitter-1 as ρ increases. The transmission loss of the device for varying ρ is dependent on L_s and α^j_{eff} as plotted in Fig. 11(c). We notice that when ρ is 1.5, the transmission losses for both devices are below 0.4 dB.

In summary we find the optimal structural parameters for our dual slotted core fibers to be $\Lambda = 40\,\mu$m, $f_A = 0.6$, $f_B = 0.404$, $\rho = 1.5$ for Splitter-1 and $\Lambda = 40\,\mu$m, $f = 0.6$ $\rho = 1.5$ for Splitter-2.

3.3 Extinction Ratio

The final key performance parameter used to evaluate the performance of a polarization splitter we examine is the extinction ratio (ER). This is defined as the power ratio between the undesired and

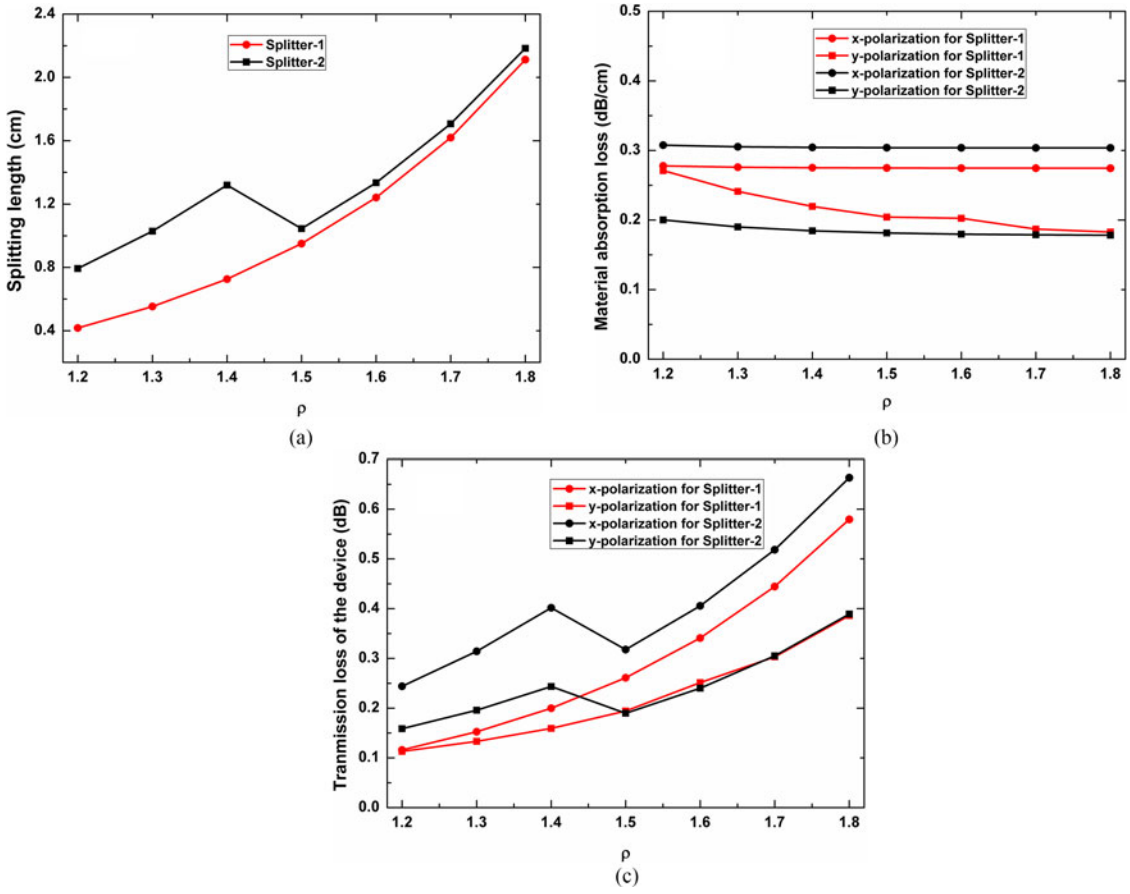

Fig. 11. (a) Splitting length, (b) material absorption loss of the four supermodes, and (c) transmission loss for x- and y-polarizations of the two splitters at 1.0 THz for varying normalized core separation ρ.

the desired polarized modes in each output core, i.e. for core A and core B, we can define the ERs as [36]

$$ER_x = 10\log_{10}\frac{P^y_{out,B}}{P^x_{out,B}} \tag{12}$$

$$ER_y = 10\log_{10}\frac{P^x_{out,A}}{P^y_{out,A}}. \tag{13}$$

Fig. 12 plots the ERs of x- and y-polarized modes as a function of the launching THz frequency for the two splitters with the optimal structural parameters discussed in the section above as well as lengths being 0.95cm for Splitter-1 and 1.023 cm for Splitter-2. For Splitter-1, the ER_x and ER_y at center frequency 1.0 THz are ~ -18 dB and ~ -90 dB, respectively. For Splitter-2, the ER_x and ER_y at center frequency 1.0 THz are both ~ -13 dB. The bandwidth of the polarization splitter is defined as the frequency range, within which the ERs of both x- and y-polarized light are better than -10 dB. From Fig. 12(a), it is clear that the ER of x-polarization for the Splitter-1 remains lower than -10 dB throughout the operational frequency range and thus, the bandwidth of Splitter-1 is determined by the bandwidth of y-polarized mode, which can be calculated to be about 0.18 THz, from 0.92 THz to 1.1 THz. The bandwidth of Splitter-2 is on the other hand the overlapped bandwidths of the two polarizations, which can be calculated to be about 0.05 THz, from 0.98 THz to 1.03 THz.

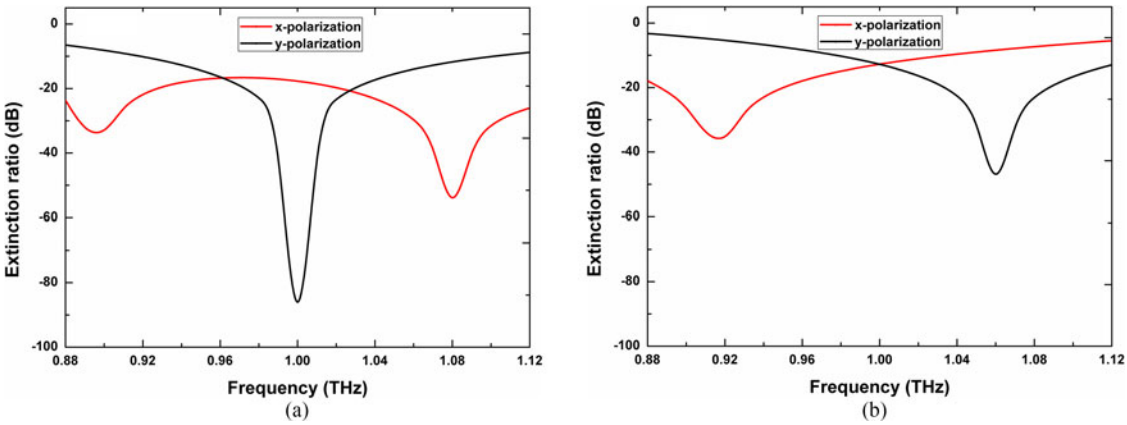

Fig. 12. Extinction ratios of x- and y-polarizations for (a) Splitter-1 and (b) Splitter-2 as a function of frequency at a fixed splitter lengths of 0.95 cm and 1.023 cm, respectively.

TABLE 1
Comparison of the Characteristics of Splitter-1 and Splitter-2

Device	Ls (cm)	Loss (dB)	BW (THz)	ER (dB)
Splitter-1	0.950	0.261(X)	0.18	−17.66(X)
		0.194(Y)		−90.66(Y)
Splitter-2	1.023	0.318(X)	0.05	−12.76(X)
		0.190(Y)		−12.77(Y)

Table 1 summarizes and compares the characteristics of the two splitters and we can see that they have comparable splitting lengths and transmission losses. Due to partial coupling behavior of the asymmetric dual core structure, x-polarized mode can be more or less completely kept almost in one core in Splitter-1, and polarization splitting can be realized by just one coupling length of the x-polarized mode. While for Splitter-2 the two polarizations can be simultaneously coupled between the two cores albeit at different coupling lengths so that selection of a particular fiber length (not necessarily the coupling length), at which the x- and y-polarized mode powers have the first difference maximum realizes polarization splitting. Thus, the near zero coupling efficiency of the x-polarization in Splitter-1 provides very low background noise for the ER of the y-polarization mode, compared to that of Splitter-2. Therefore, we can find that Splitter-1 has a broader operational bandwidth and better ERs than Splitter-2.

4. Discussion

Compared to previously reported structures [23]–[26], the two proposed based dual slotted core polymer fiber polarization splitters exhibit lower transmission losses at 0.4 dB and also are more compact, having device lengths of about 1 cm. With regards to the extinction ratio, the values of the Splitter-1 are better than the ERs in [23] and [24]; however, those of Splitter-2 are not as good as those of [25] and [26]. It should be noted that the two splitters proposed here are not suitable for broadband THz splitting systems due to the relative narrowband operation frequency however, with the emergence of the narrow linewidth terahertz sources [37] and an increasing demand in imaging

and sensing applications [3], [4], we believe that the proposed Splitter-2 has promising applicability in narrowband THz transmission systems.

From the practical point of view, the biggest challenge for these splitters is the fabrication of the proposed dual slotted core polymer fiber. Due to the non-circular air slot structure, it is difficult to control the air pressure in the fiber perform by using the traditional drawing method. However, due to the short lengths of the devices and the regular shape of the cross-section structure, some other techniques, such as the extrusion technique [38], [39] and the highly precise 3-D printing technique [40], may have potential to realize this device.

5. Conclusion

In summary, in this paper we have proposed two types of THz polarization splitters based on dual slotted core polymer fibers. Two different polarization splitting mechanisms, with partial coupling and total coupling of the two orthogonal polarizations, have been numerically investigated and compared. At 1.0 THz, with optimal structural parameters $\Lambda = 40\,\mu$m, $f_A = 0.6$, $f_B = 0.404$, and $\rho = 1.5$ for Splitter-1 and $\Lambda = 40\,\mu$m, $f = 0.6$, and $\rho = 1.5$ for Splitter-2, numerical simulations were carried out and the results show comparably short splitting lengths of about 1 cm and lower transmission losses of 0.4 dB of both structures. For Splitter-1, the index matched coupling of one polarization is realized in an asymmetric dual core structure by the ICMC method, which ensures a relatively broad operational bandwidth as compared to Splitter-2.The ERs of the x- and y-polarized modes of Splitter-1 are -18 dB and -90 dB, while those of Splitter-2 both -13dB. Overall, the performance of Splitter-1, which is based on partial coupling has better performance than that of Splitter-2, which based on total coupling. The simple structure and short lengths of the proposed splitters means that is realistic to that fabrication by using extrusion techniques or 3-D printing methods.

References

[1] B. Ferguson and X. C. Zhang, "Materials for terahertz science and technology," *Nature Mater.*, vol. 1, pp. 26–33, Sep. 2002.

[2] J. Chen, Y. Q. Chen, H. W. Zhao, G. J. Bastiaans, and X. C. Zhang, "Absorption coefficients of selected explosives and related compounds in the range of 0.1-2.8 THz," *Opt. Exp.*, vol. 15, no. 19, pp. 12060–12067, Sep. 2007.

[3] H. Chen *et al.*, "Performance of THz fiber-scanning near-field microscopy to diagnose breast tumors," *Opt. Exp.*, vol. 19, no. 20, pp. 19523–19531, Sep. 2011.

[4] D. Dragomana and M. Dragoman, "Terahertz fields and applications," *Progress Quantum Electron.*, vol. 28, pp. 1–66, 2004.

[5] A. Purkayastha, T. Srivastava, and R. Jha, "Ultrasensitive THz plasmonics gaseous sensor using doped grapheme," *Sens. Actuators B*, vol. 227, pp. 291–295, 2016.

[6] T. Kleine-Ostmann and T. Nagatsuma, "A review on terahertz communications research," *J. Infrared Millim. THz Waves*, vol. 32, pp. 143–171, 2011.

[7] A. Hassani, A. Dupuis, and M. Skorobogatiy, "Low loss porous terahertz fibers containing multiple subwavelength holes," *Appl. Phys. Lett.*, vol. 92, May 2008, Art. no. 071101.

[8] L. J. Chen, H. W. Chen, T. F. Kao, J. Y. Lu, and C. K. Sun, "Low-loss subwavelength plastic fiber for terahertz waveguiding," *Opt. Lett.*, vol. 31, no. 3, pp. 308–310, Feb. 2006.

[9] S. Atakaramians, S. V. Afshar, B. M. Fischer, D. Abbott, and T. M. Monro, "Porous fibers: A novel approach to low loss THz waveguides," *Opt. Exp.*, vol. 16, no. 12, pp. 8845–8854, Jun. 2008.

[10] J. Lu, C. Yu, H. Chang, H. Chen, Y. Li, C. Pan, and C. Sun, "Terahertz air-core microstructure fiber," *Appl. Phys. Lett.*, vol. 92, 2008, Art. no. 64105.

[11] K. Nielsen, H. K. Rasmussen, P. U. Jepsen, and O. Bang, "Porous-core honeycomb bandgap THz fiber," *Opt. Lett.*, vol. 36, no. 5, pp. 666–668, Mar. 2011.

[12] T. Srivastava, R. Das, P. Padhy, and R. Jha, "THz mode-coupling in photonic-crystal-surface-plasmon-coupled waveguides," *Appl. Phys. B*, vol. 118, pp. 387–392, 2015.

[13] S. F. Zhou, L. Reekie, H. P. Chan, Y. T. Chow, P. S. Chung, and K. M. Luk, "Characterization and modeling of Bragg gratings written in polymer fiber for use as filters in the THz region," *Opt. Exp.*, vol. 20, no. 9, pp. 9564–9571, Apr. 2012.

[14] G. F. Yan, A. Markov, Y. Chinifooroshan, S. M. Tripathi, W. J. Bock, and M. Skorobogatiy, "Resonant THz sensor for paper quality monitoring using THz fiber Bragg gratings," *Opt. Lett.*, vol. 38, no. 13, pp. 2200–2202, Jul. 2013.

[15] H. W. Chen *et al.*, "Subwavelength dielectric-fiber-based THz coupler," *J. Lightw. Technol.*, vol. 27, no. 11, pp. 1489–1495, Jun. 2009.

[16] K. Nielsen, H. K. Rasmussen, P. U. Jepsen, and O. Bang, "Broadband terahertz fiber directional coupler," *Opt. Lett.*, vol. 35, no. 17, pp. 2879–2881, Sep. 2010.

[17] L. Zhang and C. X. Yang, "Polarization splitter based on photonic crystal fibers," *Opt. Exp.*, vol. 11, no. 9, pp. 1015–1020, May 2003.
[18] L. Rosa, F. Poli, M. Foroni, A. Cucinotta, and S. Selleri, "Polarization splitter based on a square-lattice photonic-crystal fiber," *Opt. Lett.*, vol. 31, no. 4, pp. 441–442, Feb. 2006.
[19] J. H. Li, J. Y. Wang, R. Wang, and Y. Liu, "A novel polarization splitter based on dual-core hybrid photonic crystal fibers," *Opt. Laser Technol.*, vol. 43, pp. 795–800, Feb. 2011.
[20] L. Zhang and C. X. Yang, "A novel polarization splitter based on the photonic crystal fiber with nonidentical dual cores," *J. Lightw. Technol.*, vol. 16, no. 7, pp. 1670–1672, Jul. 2004.
[21] M. Y. Chen, B. Sun, Y. K. Zhang, and X. X. Fu, "Design of broadband polarization splitter based on partial coupling in square-lattice photonic-crystal fiber," *Appl. Opt.*, vol. 49, no. 16, pp. 3042–3048, Jun. 2010.
[22] S. Liu, S. G. Li, G. B. Yin, R. P. Feng, and X. Y. Wang, "A novel polarization splitter in ZnTe tellurite glass three-core photonic crystal fiber," *Opt. Commun.*, vol. 285, pp. 1097–1102, Jan. 2012.
[23] S. S. Li, H. Zhang, Y. Hou, J. J. Bai, W. W. Liu, and S. J. Chang, "Terahertz polarization splitter based on orthogonal microstructure dual-core photonic crystal fiber," *Appl. Opt.*, vol. 52, no. 14, pp. 3305–3310, May 2013.
[24] S. S. Li, H. Zhang, J. J. Bai, W. W. Liu, Z. W. Jiang, and S. J. Chang, "Dual-porous fiber-based low loss broadband terahertz polarization splitter," *IEEE Photon. Technol. Lett.*, vol. 26, no. 14, pp. 1399–1402, Jul. 2014.
[25] Y. F. Zhu, M. Y. Chen, H. Wang, H. B. Yao, Y. K. Zhang, and J. C. Yang, "Design and analysis of a low-loss suspended core terahertz fiber and its application to polarization splitter," *IEEE Photon. J.*, vol. 5, no. 6, Dec. 2013, Art. no. 7101410.
[26] Y. F. Zhu, M. Y. Chen, H. Wang, Y. K. Zhang, and J. C. Yang, "A low transmission loss THz polarization splitter based on dual-core optical fiber," *Photon. Nanostruct.–Fundam. Appl.*, vol. 12, pp. 184–188, Jan. 2014.
[27] P. D. Cunningham *et al.*, "Broadband terahertz characterization of the refractive index and absorption of some important polymeric and organic electro-optic materials," *J. Appl. Phys.*, vol. 109, May 2011, Art. no. 043505.
[28] K. S. Chiang, "Radial effective-index method for the analysis of optical fibers," *Appl. Opt.*, vol. 26, no. 15, pp. 2969–2973, Aug. 1987.
[29] V. Rastogi and K. S. Chiang, "Holey optical fiber with circularly distributed holes analyzed by the radial effective-index method," *Opt. Lett.*, vol. 28, no. 24, pp. 2449–2451, Dec. 2003.
[30] Y. F. Zhu, M. Y. Chen, and H. Wang, "A low-loss terahertz fiber with crossed rectangular shaped dielectric strips," *IEEE Trans. THz Sci. Technol.*, vol. 5, no. 5, pp. 751–760, Sep. 2015.
[31] H. W. Chen *et al.*, "Investigation on spectral loss characteristics of subwavelength terahertz fibers," *Opt. Lett.*, vol. 32, no. 9, pp. 1017–1019, May 2007.
[32] A. W. Snyder and J. D. Love, *Optical Waveguide Theory*, London, U. K.: Kluwer, 2000.
[33] A. Yariv and Y. Pochi, *Photonics: Optical Electronics in Modern Communications*, New York, NY, USA: Oxford Univ. Press, 2007.
[34] J. D. Love and A. Ankiewicz, "Modal cutoffs in single- and few-mode fiber couplers," *J. Lightw. Technol.*, vol. LT-3, no. 1, pp. 100–110, Feb. 1985.
[35] R. A. Forber and E. Marom, "Symmetric directional coupler switches," *IEEE J. Quantum Electron.*, vol. QE-22, no. 6, pp. 911–919, Jun. 1986.
[36] K. Saitoh, Y. Sato, and M. Koshiba, "Polarization splitter in three-core photonic crystal fibers," *Opt. Exp.*, vol. 12, no. 17, pp. 3940–3946, Aug. 2004.
[37] J. R. Paul, M. Scheller, A. Laurain, A. Young, S. W. Koch, and J. Moloney, "Narrow linewidth single-frequency terahertz source based on difference frequency generation of vertical-external-cavity source-emitting lasers in an external resonance cavity," *Opt. Lett.*, vol. 38, no. 18, pp. 3654–3657, Sep. 2013.
[38] Z. G. Lian *et al.*, "Nanomechanical optical fiber," *Opt. Exp.*, vol. 20, no. 28, pp. 29386–29394, Dec. 2012.
[39] H. Ebendorff-Heidepriem, T. M. Monro, M. A. van Eijkelenborg, and M. C. J. Large, "Extruded high-NA microstructured polymer optical fibre," *Opt. Commun.*, vol. 273, pp. 133–137, Jan. 2007.
[40] Z. Wu, W. R. Ng, M. E. Gehm, and H. Xin, "Terahertz electromagnetic crystal waveguide fabricated by polymer jetting rapid prototyping," *Opt. Exp.*, vol. 19, no. 5, pp. 3962–3972, Feb. 2011.